

Effects of rotation on the Lyman- α line morphology in distant galaxies

Nicolas Garavito-Camargo.¹ Jaime E. Forero-Romero²

¹ *Universidad de los Andes* ² *Uni B*

23 April 2013

ABSTRACT

Rotation is present in the gas kinematics of galaxies up to the highest redshifts. In this paper we present for the first time radiative transfer calculations that show the impact of rotation on the morphology of the Lyman α line. To this end we construct simplified models where a galaxy is modeled as an homogeneous sphere composed as an homogenous mixture of dust and hydrogen at a constant temperature. These spheres have an solid-body rotation with linear velocities at the surface in the range $0 - 300 \text{ km s}^{-1}$. We consider radiation sources both in the center of the rotating cloud and also homogeneously distributed around the sphere. We find that higher rotational velocities increase the width of each peak in the outgoing line profile while it also increases the amount of Lyman alpha photons escaping in the line center. This trends makes that for high rotational velocities and large Hydrogen optical depths the double peak of the line tends to be erased and be replaced by a single peak the lines center. This is more pronounced for radiation sources homogeneously distributed. Concerning the escape fraction we find that rotation does not have any effect, provided that all the sources are centrally emitted. However in the case of homogeneously emitted sources we measure an increase of about a factor of 2 in the escape fraction for higher rotational velocity values.

Our work shows clearly that gas rotation has a non negligible impact on the shape of the Lyman α line.

Key words: galaxies: high-redshift - galaxies: star formation - line: formation

1 INTRODUCTION

Due to the resonant nature of the Lyman alpha line, gas kinematics play an important role shaping its morphology. In the literature there has been extensive studies of outflow/inflow configurations.

In this paper we study for the first time the impact of rotation on the morphology of the Lyman α line. To isolate the effects of rotation we focus on a simple system: the gas distribution is spherical, with homogenous density and the gas rotates as a solid body.

This paper is structured as follows.

2 IMPLEMENTATION OF BULK GAS ROTATION

We implement into CLARA the simplest model whereby a sphere rotates with homogeneous angular velocity. We define a cartesian coordinate system with its origin at the center of the sphere and the rotation axis to be the z -axis, the

components in the bulk velocity field, $\vec{v} = v_x \hat{i} + v_y \hat{j} + v_z \hat{k}$, in the gas can be written as

$$v_x = -\frac{y}{R} V_{\max}, \quad (1a)$$

$$v_y = \frac{x}{R} V_{\max}, \quad (1b)$$

$$v_z = 0, \quad (1c)$$

where R is the radius of the sphere and V_{\max} is the linear velocity at the sphere's surface. The minus sign in the x -component of the velocity indicates the direction of rotation, in this case we assume that the angular velocity vector goes in the \hat{k} direction. The linear dependence of the velocity on the radial distance describes the case of constant angular velocity $\omega = V_{\max}/R$.

We take the polar angle θ that a unitary vector makes with the rotation axis as defined by the dot product $\cos \theta = \hat{u} \cdot \hat{k}$. In the Section 4 we will present in detail how the line differs at different observing angles θ .

Velocity (km s ⁻¹)	V_{\max}	0, 50, 100, 200, 300
Hydrogen Optical Depth	τ_H	10 ⁵ , 10 ⁶ , 10 ⁷
Dust Optical Depth	τ_A	0, 1
Photons Distributions		Central, Homogeneous

Table 1. Values for the varying input parameters in CLARA. Taking into account all the possible combinations for these models

3 GRID OF SIMULATED MODELS

We compute the emergent Lyman- α line for several models with different values for the maximal rotational velocity, hydrogen optical depth, dust optical depth and initial distributions of the photons with respect to the gas. There are in total 60 models with the input parameters summarized in Table 1.

4 RESULTS

The central result of this paper is summarized in Fig. ?? where we show that rotation has a considerable effect on the morphology of the emergent Lyman-alpha line both in the case where the photons are emitted at the sphere's center and when they are initialized with an homogeneous distribution all over the gas volume.

The results for these outgoing spectra are integrated over the whole sphere, meaning that all the escaping photons were taking into account regardless of the direction of the outgoing photons. Figure ?? shows how if one gives a weight to each outgoing photon according to its direction when escaping the gas distribution it is possible to detect notable differences in the spectrum for different viewing angles.

In the following subsections we quantify the trends observed in Fig. 1 and Fig. 2 as a function of the maximum rotation velocity V_{\max} and the position of the observer with respect to the rotation angle, $\mu = \cos \theta$. All the results in this section will be expressed in terms of restframe wavelength.

First we quantify the line by its full width at half maximum (FWHM) and the peak positions. In order to interpret these results we measure how the rotation affects the average number of scatterings for each Lyman-alpha photon in the simulation. This helps us to introduce the next subsection on the escape fraction in our models including dust. We conclude the section by estimating the expected line flux for top hat filters at a fixed center and varying width.

4.1 Line width and peak maxima

The first quantitative conclusion of the effect of rotation in the Lyman alpha line is that the double peaks in the line tend to broaden until they reach a single broad emission peak. This is most evident in the case of Lyman-alpha sources homogeneously distributed in the gas distributions (Fig. ?? right panel).

To quantify the line broadening we measure a modified version of the full width at half maximum (FWHM) for half of the line, $W_{1/2}$. It means that in the case of double peaked emission, $W_{1/2}$ corresponds to the width of one of the peaks,

while in the extreme case when the line is converted into a single peak, $W_{1/2}$ corresponds to half of the full width.

This definition allows us to quantify the line width both in the cases of double and single peak emission. Furthermore it has the advantage that this line width should have a direct observational correspondence to the observed line feature once the Inter-Galactic Medium (IGM) effects are taken into account, which have the central effect of strongly reducing the intensity of the blue peak of the line.

Figure 3 summarizes our findings for $W_{1/2}$ as a function of V_{\max} . The line width increases with the rotational velocity of the gas cloud. This increase can be of a factor of 2 – 3 with respect to the width with respect to the static case. This trend is conserved at all optical depths regardless of the initial source distribution.

This result includes all the outgoing photons, regardless of the position of the observer. In Figure ?? we take into account the different positions of the observer in the measurement of the half-width $W_{1/2}$. From this we conclude that observers with a line of sight perpendicular to the axis of rotation (i.e. edge-on in the case of spiral galaxy) tend to measure larger line widths than observers aligned with the rotation axis (i.e. face-on). The influence of the observer position on the line width, amounting always less than 15% of a difference with respect to the result that takes into account all the outgoing photons with the same weight regardless of the relative observer position.

The second feature in the line that we use to quantify the effect of rotation is the position of the line maxima. These provide information on the wavelength of the majority of the outgoing photons after they interact with the neutral hydrogen atoms in the gas cloud. If most of the photon escapes with a low number of scattering, its outgoing frequency will be close to its initial frequency, that is in the center of the line. On the contrary if the number of scatterings is large for the average photon, its outgoing frequency will be far from the line center. Such reasoning can be made more quantitative to understand the dependence of the peak maxima as a function of the hydrogen optical depth in the cloud [citation needed].

In Figure ?? we present the position of the maxima as a function of V_{\max} . For the photons emitted in the line center we do not find any variation in the position of the maxima in the range of explored parameter space. However in the homogeneous case we can see how the maxima goes to $x_m = 0$, meaning that the double peak is converted into a single peak.

This transition to a single peak line occurs for the systems where it becomes easier for a bulk of the photons to escape with the lowest number of scatterings possible. This can explain how the single peak stage can be achieved in the homogeneous source distribution where there is a fraction of the photons inside a photosphere region with $\tau_H \sim 1$ which allows them to escape within one scatter. Increasing the rotational velocity makes it easier for the photons in this photosphere region to escape.

In Figure ?? we present the position of the maxima as a function of the viewing angle μ for all the optical depths and rotational velocities and the two different photon distributions [FALTA LA GRAFICA].

Finally we also report on the effect of the neutral Hydrogen optical depth τ_H on the maxima position x_m Figure ??.

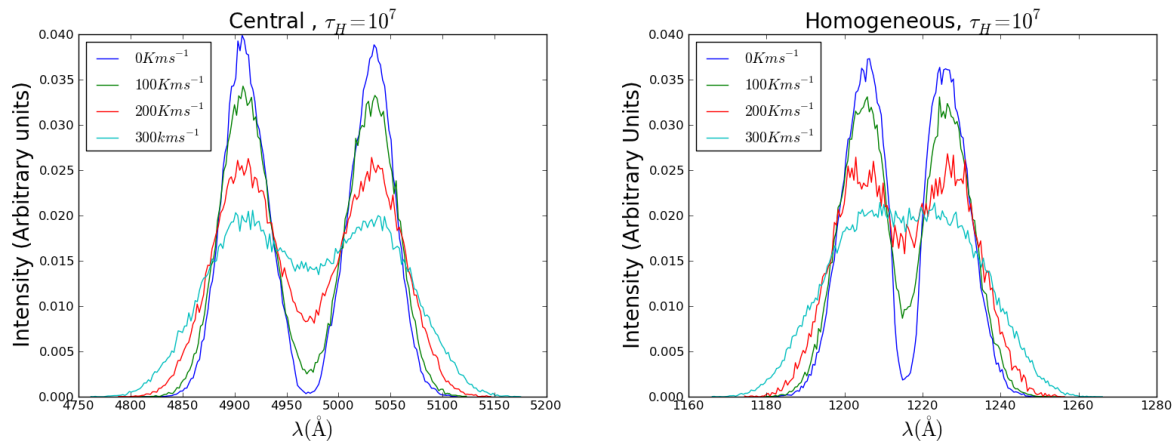


Figure 1. Shape of the Lyman alpha line for different velocities. The left (right) panel shows the central (homogeneous) photon distribution. All photons were taken into account regardless of their outgoing direction of propagation.

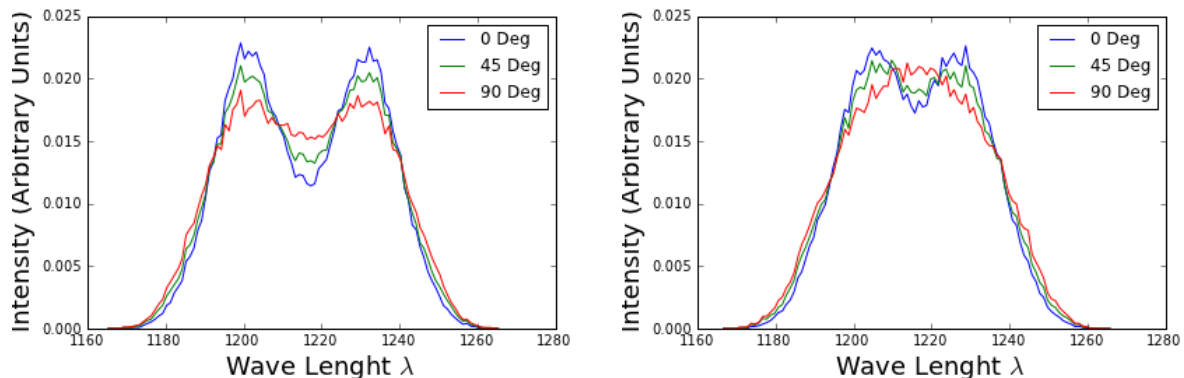


Figure 2. Same as Figure 1 but this time the different lines show the line morphology for different polar angles θ with respect to the rotation axis. In this case each photon has a weight dependent on their outgoing direction. All spectra correspond to the same $V_{\max} = 300 \text{ km s}^{-1}$, Optical Depth $\tau = 10^7$ and Central Distribution without dust.

We find that, at fixed rotation velocity, the position of the maxima increases with optical depth as expected from basic theoretical considerations. We compare our results with the expected theoretical scaling for an infinite slab.

4.2 Average Number of Scatterings

Until now we have focused on how rotation affects the morphology of the Lyman alpha line, now we turn to study deeply the possible causes of these effects. As recombination is the main cause of the Lyman alpha, it is important to study the relationship between the number of times that a photon is absorbed and re-emitted hereafter scatterings with its shift in the wavelength.

As a first approach we study the number of scatterings of all the photons at different velocities and for both distributions Figure 7. For the central distribution the number of scatterings does not change with V_{\max} , this implies that..., For the Homogeneous distribution we found that as V_{\max} increases the average number of scatterings decreases, it means that rotation..

In order to understand the double peak we make a histogram..

as we think N_{scatt} is related with the double peaked line and maxima positions.

4.3 Escape Fraction

We have seen in the previous section that rotation affects the number of scatterings that ..

Of particular interest is to compute the escape fraction of Lyman α photons coming from the most distant galaxies, due to the fact that with the observed intensity of the Lyman alpha line quantities as the LF and SFR can be derived (put some references).

Previous studies have shown the correlation of the Escape fraction with galactic mass (Lauren 2009 et al, Dayal et al 2010) abundances and the kinematics of dust. In order to study pure rotational effects in the escape fraction we fixed the dust abundance $\tau_A = 0.01$ and the galaxy mass. We compute the escape fraction for the models described

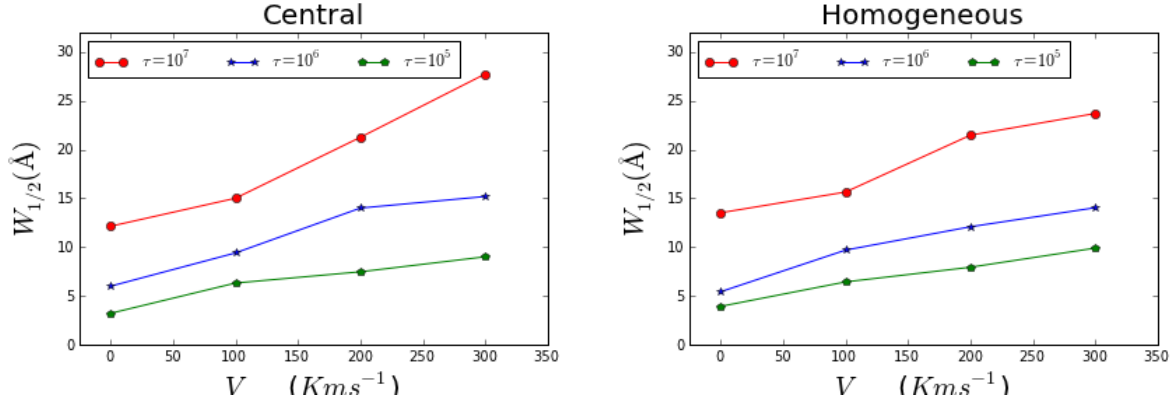


Figure 3. Width of the lyman-alpha line for all the models.

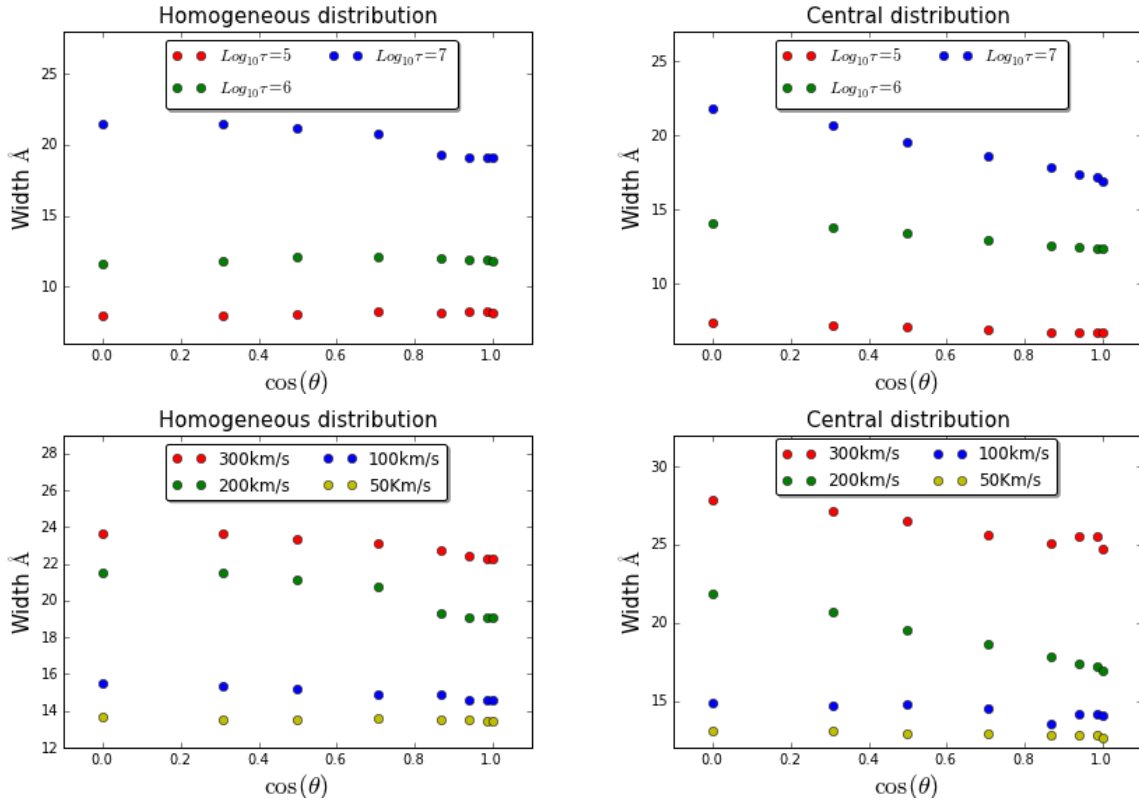


Figure 4. Width of the lyman-alpha line for all the models.

in Table 1.

For a realistic model we also take into account the viewing angle, first we fixed the viewing angle at $\theta = 0$ Fig. and then we fixed the velocity in order to see the escape fraction correlation with the viewing angle. Therefore we define the escape fraction as:

$$F_e = \frac{\sum_{NI} \vec{k} \cdot \vec{o}}{\sum_{NF} \vec{k} \cdot \vec{o}} \quad (2)$$

Where NI is the initial number of photons and NF

is the final, \vec{k} is the rotation axis direction and \vec{o} the observer direction. With this definition we compute the escape fraction for all of our models, the results are shown in Fig ??

In Figure 4.3 we found that in the central distribution the escape fraction does not change with velocity while it does in the optical depth. On the other hand for the homogeneous distribution we found that for higher velocities photons escape easily. The difference between this two results rely in the fact that in the homogeneous distribution photons are emitted closer to the escape surface and this makes this configuration more sensitive to rotation while in the central configuration the escape fraction

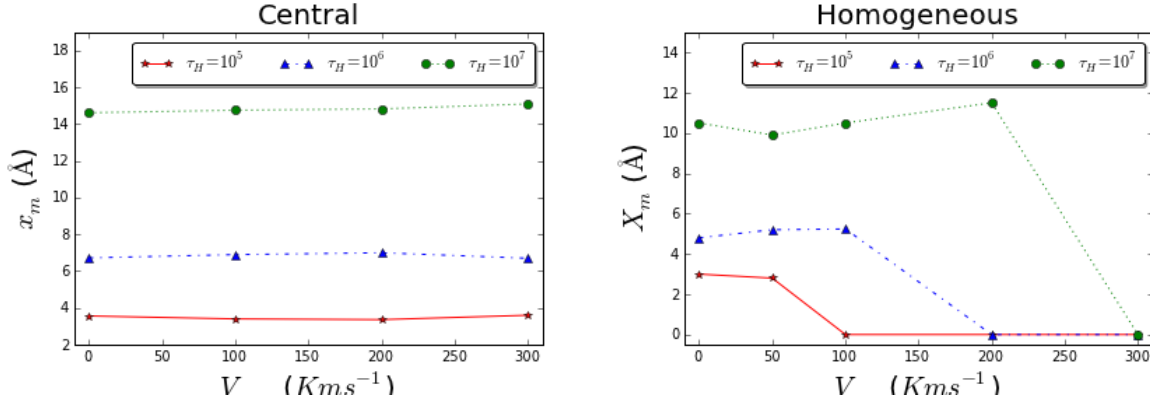


Figure 5. Position of the maxima in the outgoing spectra for different Rotational velocities, (up) Central Distribution, (Down) Homogeneous Distribution.

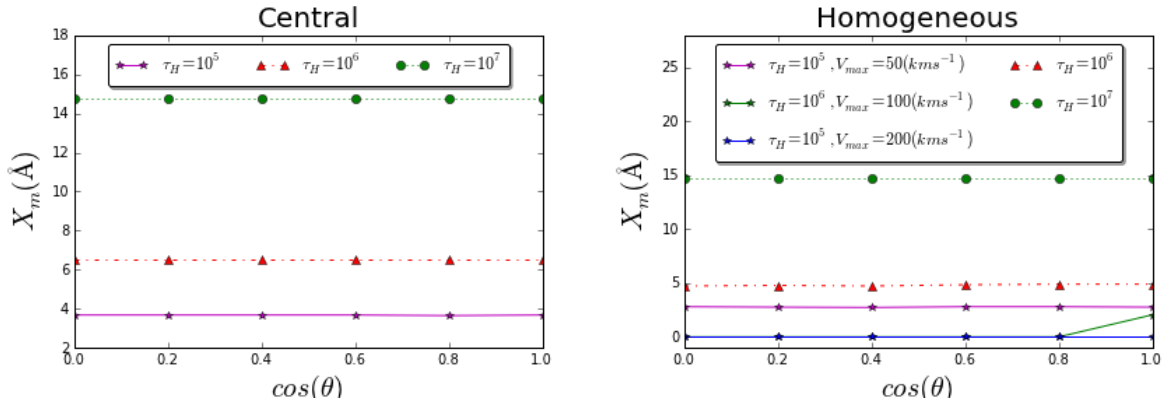


Figure 6. Position of the maxima in the outgoing spectra for different Rotational velocities, (up) Central Distribution, (Down) Homogeneous Distribution.

depends mainly in the amount of gas rather than in rotation.

Of great importance is to notest that for the homogeneous distribution the optical depth of $\tau_H = 10^5$ does not follow the trend known for the others. In order to study this FIG.(CLARA plot)

4.4 Integrated flux

5 DISCUSSION

6 OBSERVATIONAL IMPLICATIONS

... The results derived in this paper have consequences on the interpretation of galaxy observations in the Lyman alpha line.

7 CONCLUSIONS

ACKNOWLEDGEMENTS

APPENDIX A: TABLES

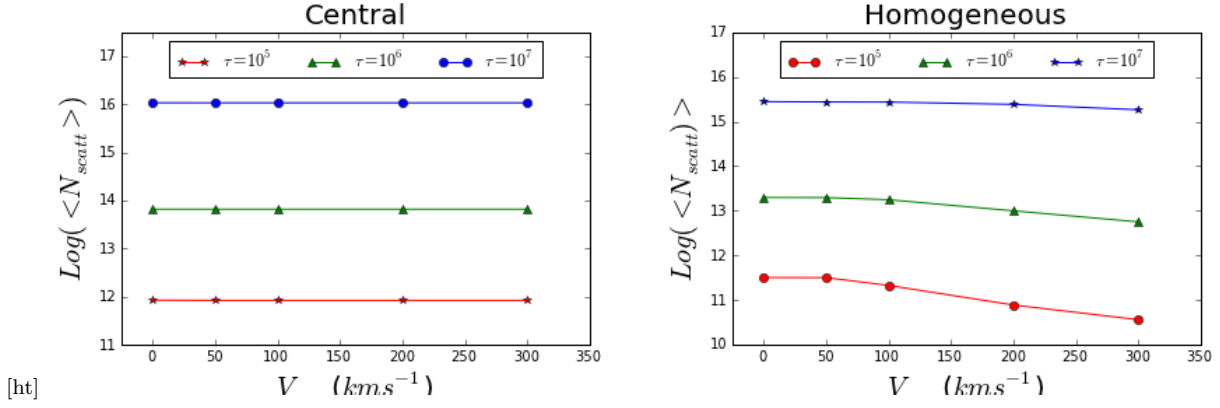


Figure 7. N_{scatt}

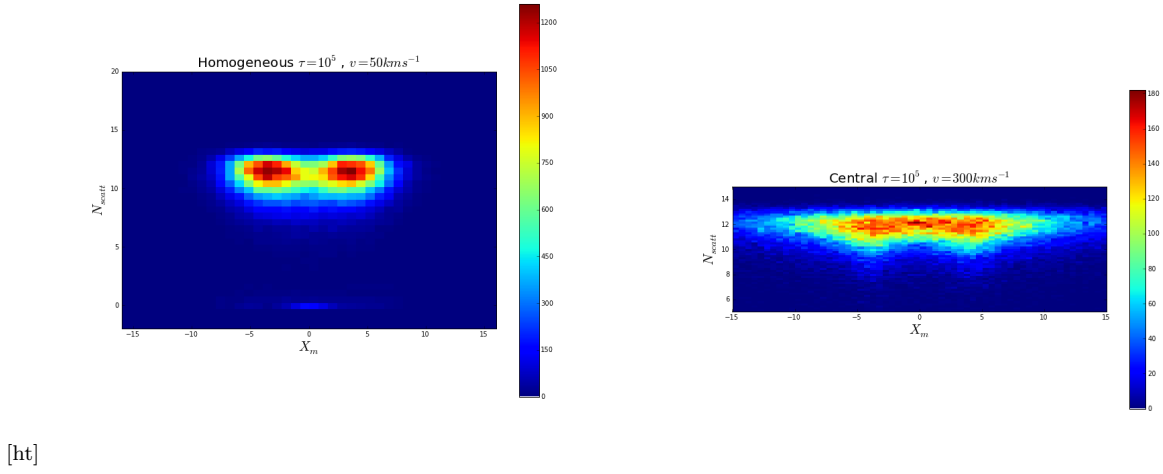


Figure 8. N_{scatt}

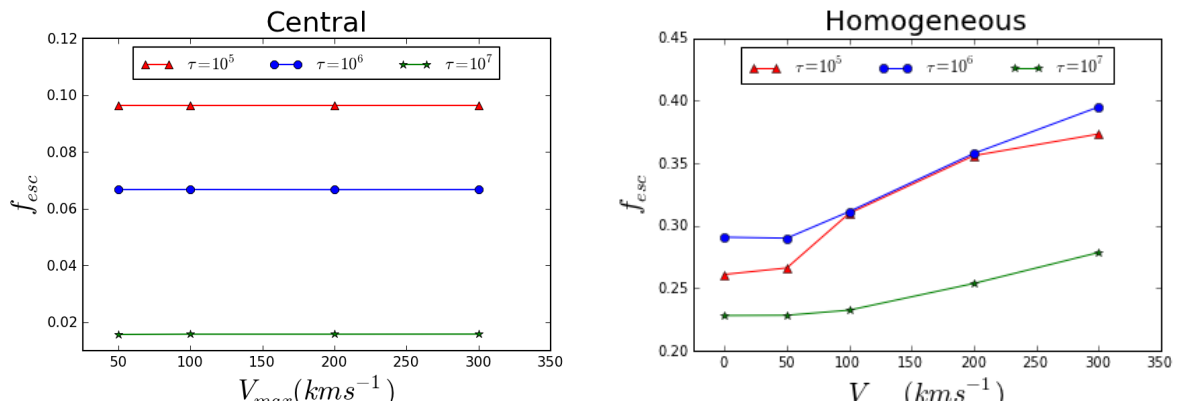


Figure 9. Escape fraction for all the models. Left panels show the central distribution, while right panels show the homogeneous distribution

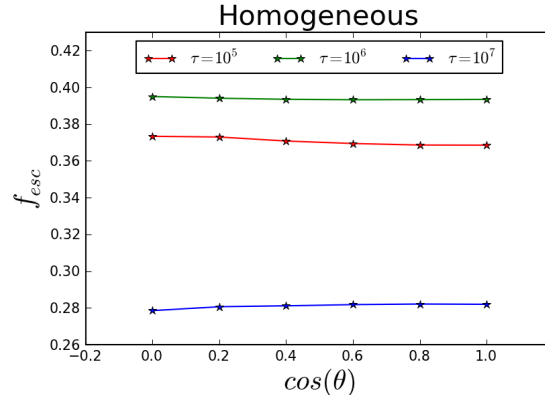


Figure 10. Escape fraction dependency with the viewing angle in the homogeneous configuration.